THE ASTROPHYSICAL JOURNAL, 237:711–733, 1980 May 1

THE H II REGION–MOLECULAR CLOUD COMPLEX W3: OBSERVATIONS OF CO, CS, AND HCN

HÉLÈNE R. DICKEL AND JOHN R. DICKEL
Department of Astronomy, University of Illinois; and Sterrewacht, Leiden
WILLIAM J. WILSON
Electronics Research Laboratory, Aerospace Corporation
AND
MICHAEL W. WERNER
Division of Physics, Mathematics, and Astronomy, California Institute of Technology
Received 1979 August 9; accepted 1979 October 22

ABSTRACT

The distributions of the emission from ^{12}CO, ^{13}CO, CS, and HCN have been mapped in the W3 molecular cloud. The emission is divided into three components according to the spatial distribution of the intensity and the associated velocity. Although the overall cloud is investigated, the emphasis is on the brightest condensation referred to as the W3 core. This dense and dynamically active region contains several embedded compact H II regions, IR sources, and masers. Strong ^{12}CO self-absorption occurs toward the compact infrared source IRS 5 where emission from dust at 1 mm and in the far-infrared and the emission from ^{13}CO and HCN are strongest, but the emission from CS, by contrast, is rather weak. Collapse of the W3 core is inferred from the line profiles. A velocity gradient is observed across the W3 core. The observations and derived physical parameters which are presented in this paper will be used in a subsequent paper to develop a model of the W3 region.

Subject headings: interstellar: molecules — nebulae: general — nebulae: individual

I. INTRODUCTION

IC 1795–W3 is a giant H II region/molecular cloud complex located in the Perseus spiral arm at $l \sim 133\overset{\circ}{.}5$. This section of the Perseus arm between $l \sim 133°$ and 137° is especially rich in star clusters—Cas OB6, Ocl 352, Ocl 364 (e.g., Ishida 1970; Hagen 1970; Alter, Ruprecht, and Vanýsek 1970), ionized hydrogen—W3, W4, and W5 (Westerhout 1958; Wendker and Altenhoff 1977; Rohlfs, Braunsfurth, and Hills 1977), and molecules—clouds associated with W3 and W5 (Dickel 1973; Wilson *et al.* 1974; Lada *et al.* 1978). The core or densest part of the W3 molecular cloud contains several embedded compact H II regions which have been studied with high spatial resolution at both near-infrared and radio wavelengths (Wynn-Williams, Becklin, and Neugebauer 1972; Wynn-Williams 1971). OH and H_2O masers have also been observed (Rogers *et al.* 1967; Goss, Lockhart, and Fomalont 1975; Genzel and Downes 1977; Forster, Welch, and Wright 1977). Figure 1 is a sketch of the W3–4 region to orient the reader and to show the general location of many of the features mentioned in this discussion.

The present study of the W3 complex began as part of our CO mapping program for which we have previously published the results for NGC 6334 (Dickel, Dickel, and Wilson 1977 [Paper I]) and W75–DR 21 (Dickel, Dickel, and Wilson 1978 [Paper II]). In this paper we present detailed observations of the CO emission in W3 which complement the CO maps of Lada *et al*, (1978) of a much larger region, including W3, W4, and W5, with lower angular resolution. In addition we have made maps of the emission from CS (J = 2–1) and HCN (J = 1–0) which arise in the denser core of the W3 molecular cloud. They allow further constraints to be placed on the derived physical parameters than is possible from the ^{13}CO and ^{12}CO data alone. The analysis of the line profiles given in this paper has allowed the development of a model of the structure and dynamics of the IC 1795–W3 complex and its relationship to the rest of the galactic environment; the model is presented in a subsequent paper (Dickel 1980).

In § II the observations are described. In § III the profiles and maps are presented, the significant observational features are discussed, and a number of physical parameters of the W3 cloud are determined. A brief summary is given in § IV.

II. OBSERVATIONS

Since the equipment and observing procedure used for these observations were described in full in Paper I, only the important parameters are repeated in Table 1.

The data consist of spectra obtained at fixed points on a grid which is centered on the group of near-infrared sources IRS 5–6–7 at $\alpha(1950) = 02^h21^m53^s$ and $\delta(1950) = +61°52'15''$. This "CENTER" position is marked by the intersection of the two inner axes drawn on most of the figures. The CO spectra of the outer parts of the W3 cloud, which were obtained with both the Aerospace and NRAO telescopes, cover

1980ApJ...237..711D

TABLE 1

OBSERVATIONAL PARAMETERS

EQUIPMENT	MOLECULE	TRANSITION	FREQUENCY (kHz)	HALF-POWER BEAMWIDTH (arcsec)	TYPICAL INTEGRATION TIME (min)	TOTAL BANDWIDTH (MHz)	RESOLUTION (kHz)	RESOLUTION (km s^{-1})	rms NOISE ON SPECTRUM (K)	ORION A T_A^* (K)
Aerospace 4.6 m, 1976.....	^{12}CO	$J=1$–0	115.271204	150	15	32.0	250	0.65	0.8	60.0
NRAO 11 m, 1973.....	^{12}CO	$J=1$–0	115.271204	70	15	12.5	250	0.65	1.0	60.0
	^{13}CO	$J=1$–0	110.201370	70	30	12.5	250	0.67	0.4	9.3
NRAO 11 m, 1974, 1975, 1976...	^{12}CO	$J=1$–0	115.271204	70	6	25.6	100	0.26	1.4	60.0
	^{13}CO	$J=1$–0	110.201370	70	10	25.6	100	0.27	0.4	9.3
NRAO 11 m, 1975.....	CS	$J=2$–1	97.981007	80	15	64.0	250	0.77	0.15	4.5 (5.9 at 2′S)
	HCN	$J=1$–0, $F=2$–1	88.631847	90	15	64.0	250	0.84	0.20	17.2

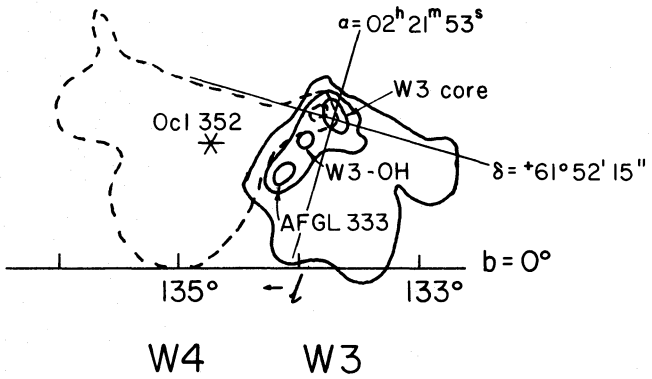

FIG. 1.—Schematic diagram of part of the Perseus spiral arm showing the location of the H II regions W3–4 (*dashed outlines*) and the associated molecular cloud (*solid line*). The stars in the OB association Cas OB6 cover the entire area. The center of the open cluster Ocl 352 which excites W4 is marked by an asterisk. The line of constant galactic latitude $b = 0°$ is drawn with tick marks every 1° in galactic longitude, and the central α, δ axes of the CO observing grid are drawn.

$\sim\frac{1}{2}°$ in α and δ with a spacing of 2′–4′ between positions. For the inner part of the W3 cloud, the spacing between points was 1′ for ^{13}CO, ^{12}CO, and CS, and somewhat larger for HCN. A finer grid, every $\frac{1}{2}'$, was used for the ^{12}CO observations in the very central region. During each observing session, the observations at the center were repeated about once each hour to correct for atmospheric extinction. The absolute calibration was provided by measuring the emission from Orion A and normalizing to the CO and HCN values taken from Ulich and Haas (1976). These are given in the last column of Table 1. Corrected antenna temperatures outside the atmosphere, T_A^*, are used throughout and are related to the brightness temperature by the forward beam efficiency which is ≥ 0.9 (Ulich and Haas 1976).

The data are presented in the following tables: Table 2A contains the ^{12}CO and ^{13}CO data for the outer regions observed at NRAO and at the Aerospace Corporation with 250 kHz resolution, Table 2B contains the ^{12}CO and ^{13}CO data for the inner regions taken at NRAO with 100 kHz resolution, and Table 3 contains the CS and HCN data obtained at NRAO with 250 kHz resolution. The layout of the tables is similar, so only Table 2A will be described in detail. The parameters in Table 2A are for the ^{12}CO lines observed with a frequency resolution of 250 kHz and a beamwidth of 2′ unless column (1) contains a footnote (c) to indicate 1′ beamwidth. A footnote (d) indicates the ^{13}CO line (all the ^{13}CO data were obtained with the 1′ resolution of the NRAO telescope). Columns (1) and (2) of the table contain the position relative to the CENTER position at $\alpha(1950) = 02^h21^m53^s$ and $\delta(1950) = +61°52'15''$. For asymmetric lines, the first row of parameters is for the main peak and the second row has a "p" or "s" in column (3) to distinguish between a secondary peak and a shoulder. Columns (4) and (5) contain the peak T_A^* and the velocity of the peak, V_p. The T_A^* and V_p for a shoulder are measured at the middle of the shoulder; no attempt has been made to divide the line into a series of overlapping Gaussian components. This is because, in at least some places, the asymmetries clearly represent self-absorption of a single profile rather than multiple components (Dickel *et al.* 1975). The integrated brightness in column (6) is for the entire profile (except in a few instances in Table 2A where individual components are separated enough to give values for each component). Because of the asymmetric profiles we have also given the velocity at the midpoint of the line, V_w, in column (7) and the full width across the profile, ΔV_w, in column (8); both quantities are measured in the line wings at the 1 K level for ^{12}CO and ^{13}CO and 0.5 K for CS and HCN. In Table 2B, columns (4)–(8) refer to ^{12}CO, and the same parameters appear in columns (9)–(13) for ^{13}CO. The spatial and frequency resolution of these observations are 1′ and 100 kHz, respectively, except where a footnote (d) appears in column (1) to indicate that the quantities were measured from profiles with 250 kHz resolution. The last three columns of Table 2B contain the following information relating to the intensity ratio of ^{13}CO to ^{12}CO across the profile: the maximum value of the ratio, max r; the velocity at which this maximum occurs, V_r; and the extent in velocity, ΔV_r, for which the ratio is $\gtrsim 0.2$. (For r less than 0.2, the velocity extent over which the ratio is $\gtrsim 0.15$ is given in parentheses.) In addition to the CO, CS, and HCN data, we have also utilized in § III*c*(ii) the 6 cm formaldehyde data for W3 published by Dickel (1973).

III. DISCUSSION OF THE MOLECULAR DATA

a) *Nomenclature*

To arrive at conclusions about various physical parameters in the complex, it is necessary to compare the present data with data in other wavelength ranges. A summary of the information available on all the important features in this complex is collected in Table 4. Although most of the entries are not new in this paper, this table is the only place where all the facts requiring explanation by a complete model of the W3 complex have been brought together. The tabular presentation is also important for sorting out the confusion in names which exist in the literature and for separating overlapping components. We shall henceforth refer to features by their designations

TABLE 2A

OBSERVATIONAL PARAMETERS FOR CO IN W3

POSITION FROM CENTER[a]		[b] (250 kHz resolution) LINE PARAMETERS					
$\Delta\alpha$ (s)	$\Delta\delta$ (arcmin)		T_A^* (K)	V_p (km s^{-1})	$\int TdV$ (K·km s^{-1})	V_w (km s^{-1})	ΔV_w (km s^{-1})
W96	S08		9.5	−41.5	63	−44.0	11.7
W96	S04		8.6	−40.0	45	−43.7	11.1
W96	N00		4.8	−42.5	25	−42.5	6.2
W86	S08		10.7	−40.3	58	−43.3	9.4
		p	8.1	−44.4			
W86	S04		6.9	−43.8	49	−42.6	8.6
		p	6.5	−40.0			
W80[c]	S05		5.6	−42.2	35	−43.1	8.6
W80	S02		6.1	−41.3	30	−41.9	7.1
W80[c]	N00		5.6	−40.7	21	−40.7	4.6
W80	N02		3.4	−44.2	10	−43.8	3.8
W64	S16		4.3	−43.5	11	−43.5	3.6
W64	S12		3.3	−44.4	14	−44.4	4.4
W64	S08		10.0	−40.4	27	−42.3	8.3
		p	3.9	−44.2	17		
W64	S04		5.4	−44.8	23	−43.2	7.4
		p	4.3	−40.3			
W64	S02		11.1	−40.0	51	−43.0	8.4
		p	6.2	−44.7			
W64	N00		6.9	−40.4	24	−43.0	8.3
		p	3.5	−44.6			
W64	N02		4.8	−44.1	21	−43.6	8.3
		p	2.4	−41.0			
W64	N04		6.7	−43.6	18	−42.9	6.2
			2.4	−41.0			
W48	S04		4.8	−45.1	27	−42.0	10.4
		p	4.8	−40.4			
		p	1.8?	−37.6			
W48	N04		4.8	−38.5	35	−41.5	11.4
		p	4.0	−44.5			
W40[c]	S10		4.2	−40.0	13	−40.2	4.2
W40[c]	S05		3.0	−43.0	24	−43.4	8.0
W40[c]	N00		9.1	−40.1	38	−42.3	11.4
		s	3.4	−44.1			
W40[d]	N00		4.1	−39.6	10	−38.6	6.0
		s	1.8	−36.5			
W40[c]	N02		8.4	−39.0	50	−42.9	12.8
		p	4.0	−46.3?			
W40[c]	N05		4.5	−44.3	36	−42.7	13.1
		p	3.6	−38.8			
W32	S16		5.3	−43.5	12	−43.4	3.1
W32	S12		1.7	−42.6	7	−42.6	3.9
W32	S08		4.1	−43.2	15	−41.6	7.3
		p	2.0	−40.3			
W32	S04		13.2	−41.0	45	−41.0	5.7
W32	N04		11.5	−37.8	77	−41.7	13.9
		p	6.5	−41.0			
		p	4.7	−44.9			
W24[c]	S03		10.3	−41.9	41	−41.6	6.5
W24[c]	N00		18.0	−40.8	99	−41.4	11.0
W24[c]	N03		9.6	−39.5	54	−40.4	9.8
		s	5.4	−42.9			
W16	S04		6.2	−41.0	21	−40.6	6.0
		s	3.3	−39.1?			
W16	N04		10.6	−40.7	57	−41.5	11.6
		s	3.5?	−46.2			
W16[c]	N07		3.0	−41.4	19	−41.2	7.0
W09[c]	N01		31.0	−43.3	233	−43.9	15.3
		s	19.0	−46.7			
		s	12.4	−39.5			
W09[d]	N01		7.4	−43.1	30	−42.3	9.3
		s	4.3	−39.5			
W08[e]	N0.5		30.0	−42.0	244	−41.8	17.0
E00	S16		10.2	−43.6	24	−43.1	4.6
E00	S12		11.3	−43.6	24	−42.4	5.7
		s	2.1	−40.9			
E00	S08		7.4	−43.1	25	−42.1	6.2
		s	3.7	−40.8			
E00[c]	S05		2.4	−40.0	18	−39.8	4.4
E00	S04		5.1	−37.8	21	−39.3	7.9
		s	3.6	−41.0			

TABLE 2A—*Continued*

Position from Center[a]		[b] (250 kHz resolution) Line Parameters					
$\Delta\alpha$ (s)	$\Delta\delta$ (arcmin)		T_A^* (K)	V_p (km s^{-1})	$\int TdV$ (K·km s^{-1})	V_w (km s^{-1})	ΔV_w (km s^{-1})
E00[c]	S02		7.9	−38.0	48	−39.0	10.4
E00[a,c,f]	N00		25.7	−41.6	203	−40.0	17.6
		p	17.8	−36.6			
E00[a,d]	N00		6.2	−39.0	27	−39.2	9.2
E00[c]	N02		16.0	−40.8	76	−41.3	9.5
E00	N04		17.8	−40.2	86	−41.1	11.8
		s	2.5	−46.2			
E00[c]	N05		7.9	−40.6	46	−42.2	8.9
		s	4.6	−43.2			
E00	N08		3.9	−41.7	19	−41.6	6.4
E04[d]	N01		3.8	−39.0	19	−39.6	10.3
E16	S04		9.3	−38.1	31	−38.2	6.9
		s	2.6	−40.7			
E16	N04		17.5	−40.4	87	−39.9	8.1
E16	N10		≤1.3	−42.6	4	−42.7	1.5
E24	S16		4.4	−44.4	17	−45.0	5.8
		p	1.6	−47.0			
E24	S12		5.3	−41.8	27	−42.5	8.3
		p	1.5	−48.8	3	−49.1	2.3
E24	S08		2.1	−36.4	3	−36.4	1.4
E24[c]	S03		13.8	−39.4	40	−39.4	6.5
E24[c]	S00		13.7	−39.6	67	−40.2	8.0
E24[d]	S00		2.5	−38.4	8	−38.6	4.3
E24[c]	N03		19.3	−40.6	79	−40.4	6.6
E24[c]	N07		10.5	−41.7	47	−41.5	7.3
E32	S04		7.9	−38.6	30	−39.1	6.0
		s	1.6	−41.0			
		p	1.5?	−45.2	3	−45.2	1.6
		p	1.5?	−31.6	3	−31.6	2.1
E32	N10		3.8	−42.9	17	−41.1	6.2
		s	2.9	−39.1			
		p	1.6?	−34.0	4	−34.0	2.6
E40[c]	S10		≤1.5				
E40[c]	S05		5.1	−39.5	14	−39.5	4.5
E40[c]	N00		13.6	−39.8	57	−40.1	8.4
E40[d]	N00		4.2	−39.0	11	−39.0	3.5
E40[c]	N02		12.4	−39.6	62	−39.6	7.8
E40[c]	N05		12.3	−41.2	41	−40.6	7.3
E40[d]	N05		2.1	−41.8	8	−41.5	2.3
E48	S16		4.6	−43.7	19	−44.5	8.2
		p	2.4	−47.0			
E48	S14		7.0	−43.4	35	−43.4	10.4
E48	S12		7.0	−43.4	37	−45.0	8.8
		p	1.0	−48.0			
E48	S04		5.4	−39.4	20	−40.4	4.7
		s	1.6?	−41.6			
		p	1.4?	−30.3	4	−30.2	2.5
E47[c]	S02		10.9	−40.6	39	−40.5	6.8
E47[d]	S02		1.6	−39.2	4	−38.9	3.7
E48	N00		20.6	−39.1	72	−38.1	8.6
		s	6.3	−36.0			
E48	N04		10.5	−40.2	55	−39.4	10.0
		s	5.7	−37.3			
E56[c]	S01		8.1	−40.0	38	−37.8	10.2
			5.5	−34.9			
E56[c]	N03		10.4	−39.1	50	−39.4	6.9
E56[c]	N07		8.5	−42.2	39	−41.8	6.9
E64	S08		6.5	−45.6	22	−45.8	5.4
E64	N00		9.3	−38.6	62	−39.9	14.9
		p	6.0	−35.4			
		p	3.1	−44.2			
E64	N02		14.1	−38.6	53	−39.7	10.0
		p	4.3?	−35.5			
		p	2.1	−42.6			
E64	N04		9.6	−38.8	47	−39.9	8.8
			4.8	−36.7			
			4.8	−42.7			
E74[d]	N09		≤1.6	−39.2	8	−39.6	8.4
E76	S17		15.8	−47.4	78	−46.5	7.8
		p	11.3	−44.9			
E80[c]	S15		11.2	−47.2	75	−46.3	11.9

TABLE 2A—*Continued*

Position from Center[a]			[b](250 kHz resolution) Line Parameters				
$\Delta\alpha$ (s)	$\Delta\delta$ (arcmin)		T_A* (K)	V_p (km s^{-1})	$\int TdV$ (K·kms^{-1})	V_w (km s^{-1})	ΔV_w (km s^{-1})
E80[d]	S15		5.0	−47.4	25	−46.4	7.9
E80[c]	S10		11.7	−46.8	70	−47.1	8.6
E80[d]	S10		4.3	−44.6	7	−44.7	1.9
E80	S08		12.7	−46.0	63	−46.5	8.6
		s	5.8	−49.5			
E80[c]	S05		5.3	−46.8	30	−44.6	11.2
		s	3.9	−41.2			
E80	S02		5.5	−46.2	19	−44.5	6.1
		s	4.3	−43.4			
E80	N00		5.9	−45.9	45	−41.0	13.2
		p	4.4	−43.8			
		p	2.2	−38.8			
E80[c]	N05		4.1	−40.5	25	−38.8	8.1
E80[c]	N10		5.4	−43.1	17	−43.6	4.8
E84[c]	S13.5		17.6	−48.6	120	−47.4	14.3
E84[d]	S13.5		5.5	−47.5	27	−47.4	6.6
E94	S17		10.2	−47.5	45	−46.5	8.0
		p	2.8	−43.9			
E96	S08		12.7	−47.5	63	−47.4	7.1
E112	S08		3.0	−47.4	15	−47.5	5.7

[a] Center at $\alpha(1950) = 02^h21^m53^s$, $\delta(1950) = +61°52'15''$.
[b] ^{12}CO Aerospace data with 2′ beam (but see exceptions in footnotes c, d below).
[c] ^{12}CO NRAO data with 1′ beam.
[d] ^{13}CO NRAO data with 1′ beam.
[e] Average of 10 scans.
[f] Average of 11 scans.

in column (1) of this table. A brief description follows in column (2), other names of the object and/or associated emission are listed in column (3), and the position of the component in galactic and equatorial coordinates is tabulated in columns (4) and (5). Pertinent references for the entries in column (3) are given in the last column.

The overall W3–W4 region is sketched in Figure 1. A reproduction of the red Sky Survey print of the W3 area is in Figure 2, and the "northern group" of sources is portrayed in Figure 3.

b) Large-Scale Features

i) *The Association of the W3 Molecular Cloud with the W4* H II *Region*

The distribution of the ^{12}CO emission in the W3 area is shown overlaid on the Palomar Sky Survey red print in Figure 2*a*. For comparison, a map of the radio continuum emission from the W3 region at 49 cm made with the Westerbork Synthesis Radio Telescope (WSRT) by Harten (1980) is shown in Figure 2*b*. Only the brightest parts of the CO cloud are shown down to $T_A^* \geq 2$ K. Low-level emission ($T_A^* < 10$ K) extends over 3 square degrees (Lada *et al.* 1978) and stops abruptly where it encounters the western ionization front of the W4 H II region (part of which is seen in the lower left of Fig. 2 to the east of $\alpha \sim 2^h25^m$). *Because of the similar distance of* ~2 kpc *for the exciting stars of the W3 and W4* H II *regions* (Ishida 1969, 1970; Ogura and Ishida 1976) *and the apparent interaction of the W3 molecular cloud with the W4* H II *region, it is concluded that the W3 molecular cloud and the W4* H II *region are in physical contact.*

ii) *Regions of Enhanced* CO *Intensity*

Our CO data show that the emission from the W3 cloud is strongest toward regions of enhanced density and/or temperature as indicated by the presence of embedded compact H II regions, near-infrared sources, and masers. The strongest CO emission occurs in the main "W3 core," whose central part coincides with the strongest radio continuum emission (compare Figs. 2*a* and 2*b*). A second such region of enhanced CO emission is along the border with W4 and includes the W3–OH maser at $\alpha \sim 2^h23^m3$, $\delta \sim 61°39'$. There is a small enhancement of the radio continuum emission along this ridge (Wendker and Altenhoff 1977). (Another source along this border, AFGL 333 at $\alpha \sim 2^h24^m6$ and $\delta \sim 61°14'.7$, has been observed in CO by Lada *et al.* 1978). The remaining weak CO emission may be considered as a third component of the W3 molecular cloud.

iii) *Velocity Structure*

The CO emission can also be divided into the three distinct regions discussed above according to its velocity as shown in Figure 2*a*: the brightest part of the W3 molecular cloud, "W3 core," has a velocity referred to the local standard of rest of $\sim -40.5 \pm 2.5$ km s^{-1}; the region along the W4 ionization front has a radial velocity of $\sim -47 \pm 2$ km s^{-1}; and the

1980ApJ...237..711D

TABLE 2B

OBSERVATIONAL PARAMETERS FOR ^{12}CO AND ^{13}CO FOR INNER PART OF W3

POSITION FROM CENTER[a]		^{12}CO (100 kHz resolution) LINE PARAMETERS					^{13}CO (100 kHz resolution) LINE PARAMETERS					max r = maximum $\frac{T_A^*(^{13}CO)}{T_A^*(^{12}CO)}$	V_r	FOR $r \geq 0.2$ ΔV_r
$\Delta\alpha$ (s)	$\Delta\delta$ (′)	T_A^* (K)	V_p (km s^{-1})	$\int TdV$ (K km s^{-1})	V_w (km s^{-1})	ΔV_w (km s^{-1})	T_A^* (K)	V_p (km s^{-1})	$\int TdV$ (K km s^{-1})	V_w (km s^{-1})	ΔV_w (km s^{-1})		(km s^{-1})	(km s^{-1})
W42	S02	8.3	−41.2	21	−40.3	4.2								
W34	S01	11.7	−40.4	47	−40.4	7.5	3.6	−40.0	8	−39.9	2.6	0.31	−40.0	2.0
W34	N00	12.8	−40.0	58	−40.0	7.9	4.4	−40.0	13	−39.4	4.9	0.32	−40.0	4.0
	s	8.5	−38.0				1.5	−37.7						
W34	N01	14.1	−40.0	56	−39.7	9.3	3.2	−40.0	10	−39.5	3.6	0.25	−39.5	1.0
W34	N02	10.8	−39.4	44	−39.6	6.4	2.3	−39.0	6	−39.0	3.1	0.25	−38.5	0.5
W25	S02	14.3	−41.6	62	−41.1	9.3	1.6	−41.0	6	−41.0	3.2	0.17	−39.8	(0.5)
W25	S01	17.6	−41.0	97	−41.6	10.0	3.1	−40.0	13	−40.4	5.0	0.22	−38.5	2.0
W25	N00	18.4	−40.5	110	−41.6	11.1	4.0	−40.5	20	−40.2	6.8	0.23	−38.8	4.0
W25	N01	15.1	−39.7	51	−40.8	7.5	2.1	−39.6	6	−39.5	3.0	0.14	−39.7	
W25	N02	12.7	−39.7	76	−41.0	9.6	3.2	−38.9	10	−40.0	6.0	0.28	−38.8	1.5
	s	7.5	−42.5				1.1	−42.4						
W25	N03						3.9	−38.8	11	−40.0	5.5			
	s						1.9	−41.0						
W17	S02	8.9	−41.5	36	−41.6	8.7	1.1	−39.7	5	−39.3	2.2	0.20	−39.7	1.5
W17	S01	19.8	−41.0	78	−41.1	7.7	3.2	−40.5	17	−41.2	5.2	0.22	−39.7	1.5
W18	S0.5	27.5	−42.0	222	−42.9	16.2								
	s	17.1	−39.2											
W17	N00	25.6	−42.5	144	−41.5	11.0	5.1	−41.0	28	−40.8	8.8	0.35	−40.0	5.0
W18	N0.5	20.7	−41.8	126	−42.5	12.1								
	s	15.3	−39.2											
W17	N01	18.8	−42.5	95	−41.4	13.2	3.2	−42.2	22	−41.0	7.0	0.24	−38.8	5.5
W17	N02	13.0	−40.5	83	−41.8	12.0	1.5	−39.1	16	−39.3	7.0	0.17	−39.0	(2.0)
W17	N03	14.7	−40.0	59	−40.4	9.3	2.0	−38.5	7	−39.4	4.0	0.20	−38.2	1.5
	s	9.8	−38.0				1.6	−40.5						
W08	S02	6.8	−41.2	32	−40.8	6.3	1.3	−39.2	5	−39.8	5.0	0.25	−38.5	3.0
W08	S01	16.8	−39.8	99	−40.8	15.0	4.4	−40.2	21	−39.8	5.2	0.30	−39.7	3.5
W08	N00	30.5	−42.2	226	−41.2	19.5	5.7	−41.8	46	−41.8	9.8	0.33	−39.7	7.0
W09	N0.5	29.7	−43.5	265	−42.9	16.2								
	s	15.9	−39.2											
W08	N01	31.0	−43.7	241	−43.0	14.0	4.6	−43.0	26	−41.5	9.0	0.15	−43.0	(1.0)
	s	13.0	−38.8				2.3	−39.3				0.20	−39.2	1.0
W08	N01	31.0	−43.0	276	−42.5	19.6	4.8	−43.8	34	−42.4	10.2	0.16	−43.5	(1.5)
	s	18.0	−39.0				2.7	−39.6				0.16	−38.5	(1.0)
W09	N1.5	15.9	−41.4	123	−42.2	13.2								
W08	N02	13.9	−43.5	97	−42.5	13.2	1.7	−40.5	10	−40.5	6.0	0.15	−41.0	(2.0)
	s	12.0	−40.3											
W08	N03	10.9	−40.7	41	−41.2	8.0	2.3	−40.5	7	−40.5	1.5	0.28	−40.0	1.5
W02	N00	30.2	−41.8	254	−41.1	20.8								
	s	20.0	−45.2											
E00	S03	3.7	−40.0	26	−40.3	9.7								
E00	S02	5.1	−39.1	33	−39.3	13.2	1.5	−38.8	6	−38.2	1.5	0.25	−38.8	0.5
E00	S01	14.4	−39.4	96	−39.8	12.5	6.1	−38.0	21	−38.2	8.8	0.55	−38.0	7.0
E00[a]	N00	25.6	−41.3	212	−39.7	17.8	6.8	−39.2	28	−39.5	10.0	0.44	−38.7	4.0
	s	21.4	−36.0											

TABLE 2B—*Continued*

Position from Center[a]		^{12}CO (100 kHz resolution) Line Parameters					^{13}CO (100 kHz resolution) Line Parameters					max r = maximum $\frac{T_A^*(^{13}CO)}{T_A^*(^{12}CO)}$	V_r	For $r \geq 0.2$ ΔV_r
$\Delta\alpha$ (s)	$\Delta\delta$ (′)	T_A^* (K)	V_p (km s^{-1})	$\int TdV$ (K km s^{-1})	V_w (km s^{-1})	ΔV_w (km s^{-1})	T_A^* (K)	V_p (km s^{-1})	$\int TdV$ (K km s^{-1})	V_w (km s^{-1})	ΔV_w (km s^{-1})		(km s^{-1})	(km s^{-1})
E00[a,b]	N00	25.8	−41.2	212	−38.6	24.0	6.2	−38.9	22	−38.9	7.6	0.38	−38.5	3.0
		s 21.6	−36.3											
E00	N0.5	24.7	−40.6	168	−40.3	17.4								
		s 8.1	−45.2											
E00	N01	23.2	−40.7	161	−41.5	14.5	3.4	−39.3	20	−40.8	7.2	0.16	−39.5	(6.0)
		s 12.2	−45.0				1.3	−44.5						
E00	N02	15.4	−40.3	74	−42.3	11.2	1.7	−41.5	10	−41.5	3.0	0.20	−42.5	1.0
		s 3.4	−45.0											
E00	N03	8.5	−40.3	37	−40.2	6.2	1.9	−39.3	7	−39.3	4.2	0.22	−39.7	1.0
E08	S02	15.4	−39.0	75	−39.7	10.2	4.2	−38.3	12	−39.8	4.5	0.30	−38.0	1.5
[c]		≤1.0	−23.3	3	−23.5	2.8								
E08	S01	18.3	−39.5	91	−38.0	9.5	5.3	−39.7	18	−38.1	5.3	0.36	−38.0	4.0
E08	N00	24.4	−40.3	149	−38.6	14.8	4.9	−38.3	18	−39.2	6.2	0.33	−38.0	2.0
		20.7	−37.2											
E08	N01	23.2	−40.8	100	−39.5	9.0	2.5	−39.0	11	−39.2	4.5	0.20	−38.0	0.5
E08	N02	15.4	−39.5	62	−40.5	8.0	2.1	−40.0	11	−40.7	6.2	0.18	−40.0	(4.0)
E08	N03	21.8	−39.8	88	−40.0	10.0	2.8	−39.2	11	−38.9	4.2	0.19	−39.0	(1.0)
		2.6	−44.5?				0.7?	−43.0						
E17	S05	≤1.8	−40.0				< 0.4	−39.0						
[c]		3.7	−22.6	4	−22.6	2.7	≤0.8	−22.4	≤1			≤0.1		
E17	S02	14.6	−38.8	58	−38.8	7.2	5.3	−39.2	17	−39.2	5.0	0.35	−38.8	5.0
[c]		≤1.0	−22.8											
E16	S01	17.3	−39.5	91	−39.8	11.2	5.7	−39.8	16	−39.8	3.8	0.37	−38.5	2.0
E17	N00	21.4	−39.7	99	−39.8	8.5	4.5	−38.6	13	−38.8	4.5	0.30	−38.0	2.5
E17	N01	20.7	−39.4	94	−40.3	8.0	3.2	−38.8	8	−38.6	2.2	0.19	−38.5	1.0
E17	N02	20.7	−40.0	80	−40.8	7.5	4.9	−39.0	15	−39.0	4.0	0.30	−38.5	2.5
E17	N03	17.5	−39.6	75	−39.5	7.5	4.4	−39.6	13	−39.5	4.5	0.23	−39.8	1.5
E17	N05	10.7	−40.8	54	−41.2	7.8	4.7	−41.2	12	−40.8	3.8	0.35	−41.0	4.0
E24	S02	18.7	−38.5	69	−39.2	8.0	3.8	−38.5	8	−38.7	3.0	0.21	−38.5	1.0
[c]		≈0	−23.0											
E24	S01	18.3	−39.2	60	−39.2	6.8	4.8	−39.5	11	−39.2	3.5	0.25	−39.7	2.0
E25	N01	9.9	−38.5	41	−39.5	6.4	1.8	−39.5	5	−39.6	3.0	0.18	−40.0	(2.0)
E25	N02	13.6	−39.5	60	−39.6	8.4	2.9	−40.0	11	−39.7	4.5	0.20	−39.8	1.5
E25	N03	19.5	−40.2	83	−39.7	8.2	2.4	−39.2	11	−39.4	4.9	0.15	−38.8	(0.5)
E34	N04	15.0	−41.3	58	−40.2	7.0	1.3	−40.5	3	−40.6	1.0	0.11	−40.0	
E42	S02	17.1	−39.5	52	−39.0	6.0								
[c]		< 1.0	−23.0											
[c]		< 1.0	−34.0											
E42	N07	15.1	−41.7	52	−41.2	7.0	2.7	−41.0	9	−41.2	3.5	0.25	−40.5	1.0
E59[c]	S05	3.7	−33.7	3	−33.2	4.8								
E59	N9.5	11.5	−42.8	38	−43.1	5.0								
E59	N11.5	10.5	−42.8	28	−43.2	4.2								
E68[c]	S03	2.2	−45.2	7	−45.2	1.8								
		s 1.2	−39.0		−35.7	2.0								
		< 0.6	−34.0											

TABLE 2B—*Continued*

Position from Center[a]		^{12}CO (100 kHz resolution) Line Parameters					^{13}CO (100 kHz resolution) Line Parameters					max r = maximum $\frac{T_A^*(^{13}CO)}{T_A^*(^{12}CO)}$	V_r (km s^{-1})	For $r \geq 0.2$ ΔV_r (km s^{-1})
$\Delta\alpha$ (s)	$\Delta\delta$ (′)	T_A^* (K)	V_p (km s^{-1})	$\int TdV$ (K km s^{-1})	V_w (km s^{-1})	ΔV_w (km s^{-1})	T_A^* (K)	V_p (km s^{-1})	$\int TdV$ (K km s^{-1})	V_w (km s^{-1})	ΔV_w (km s^{-1})			
E74	S15	12.9	−45.7	52	−46.2	11.0								
E74	S13	15.9	−45.2	115	−45.0	11.0	3.6	−46.0	12	−45.7	4.7	0.25	−46.	1.0
E74	S11	11.5	−44.8	48	−44.6	8.8								
E76	N07	8.1	−41.8	24	−40.5	6.0	≤0.8					≤0.06		
E76	N9.5	7.8	−42.2	32	−42.0	8.0	≤1.0	−43.0	2	−42.8	3.0	0.14	−43.0	
E76	N11.5	6.8	−42.7	17	−42.7	3.5	≤1.0	−42.7	2	−42.7	1.0	≤0.20	−42.7	(2.0)
E92	S15	14.9	−47.3	74	−46.0	9.5	3.4	−47.0	11	−47.2	3.2	0.23	−46.8	1.5
E92	S13	19.5	−48.3	117	−48.4	13.2	5.3	−47.8	16	−48.0	5.0	0.30	−47.7	2.0
E92	S11	19.3	−48.5	76	−47.2	8.5	2.7	−48.2	11	−46.6	5.2	≤0.20	−48.2	(0.5)
	s	6.1	−45.0				1.3	−45.5				0.20	−45.2	2.5
E94[c]	N07	2.4	−41.0	10	−41.7	6.5								
E94	N9.5	3.2	−41.2	16	−41.6	6.2								
E94	N11.5	5.5	−42.7	9	−42.1	3.2								
E111	S15	4.6	−47.5	14	−48.5	7.5								
E111	S13	3.2	−48.7	22	−47.2	9.0	≤0.8	−47.7	≤4			≤0.25	−47.5	≤1.0
	p	1.8	−43.0											
E111	S11	6.8	−48.3	16	−47.2	4.5								

[a] Center at $\alpha(1950) = 02^h21^m53^s$, $\delta(1950) = +61°52'15''$.

[b] ^{12}CO average of 11 scans, ^{13}CO average of 13 scans.

[c] 250 kHz resolution.

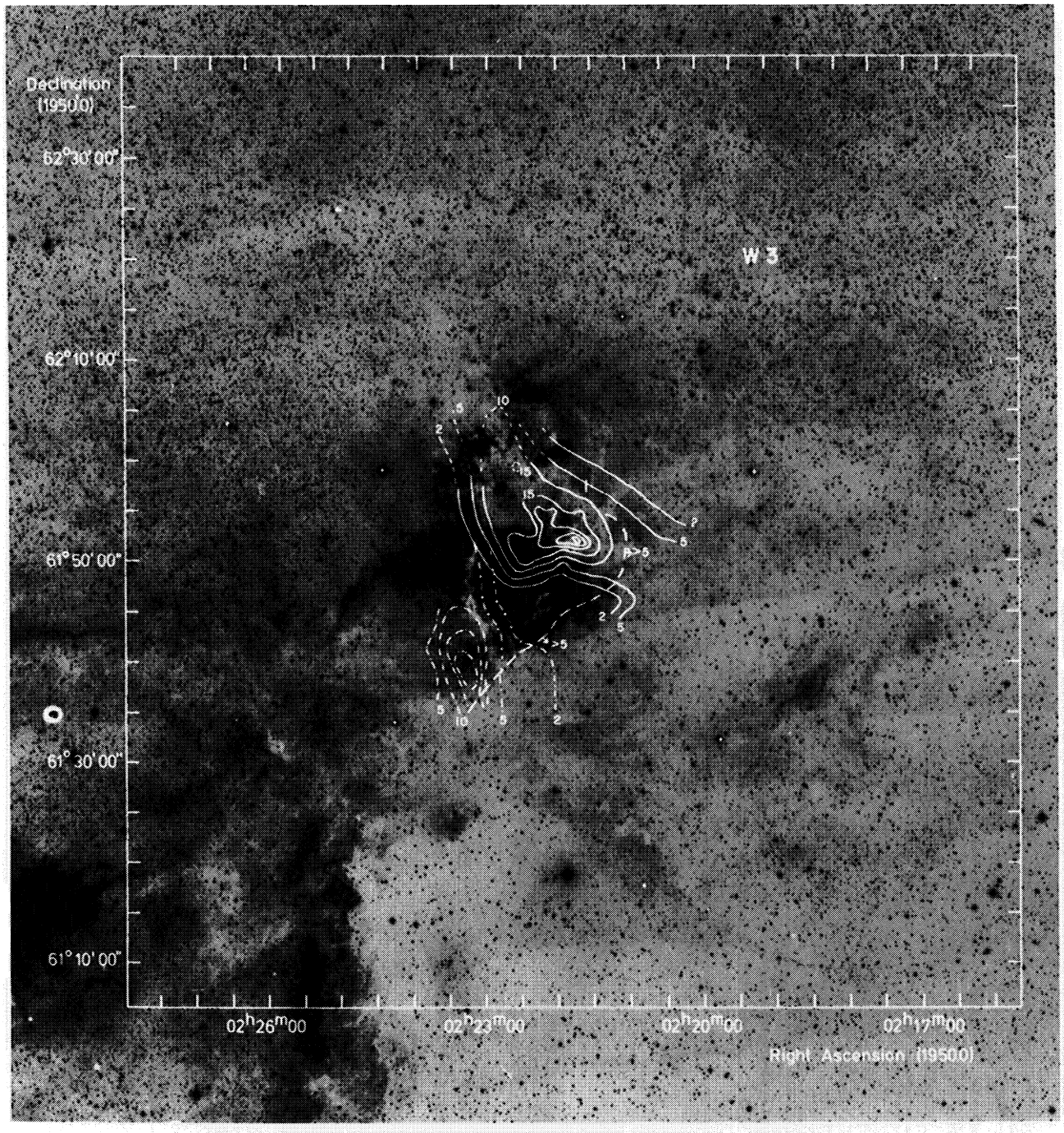

FIG. 2.—Composite pictures of the W3 region. The background is a reproduction of the red Sky Survey print courtesy of the Hale Observatories, with the following overlays: (*a*) Map of the ^{12}CO emission: Units are corrected antenna temperature with solid lines for mean radial velocities (referred to the local standard of rest) between -38 and -42 km s^{-1}, dashed lines for radial velocities between -42 and -44 km s^{-1} and dot-dashed lines for radial velocities between -45 and -49 km s^{-1}. Above 5 K, the contour interval is 5 K.

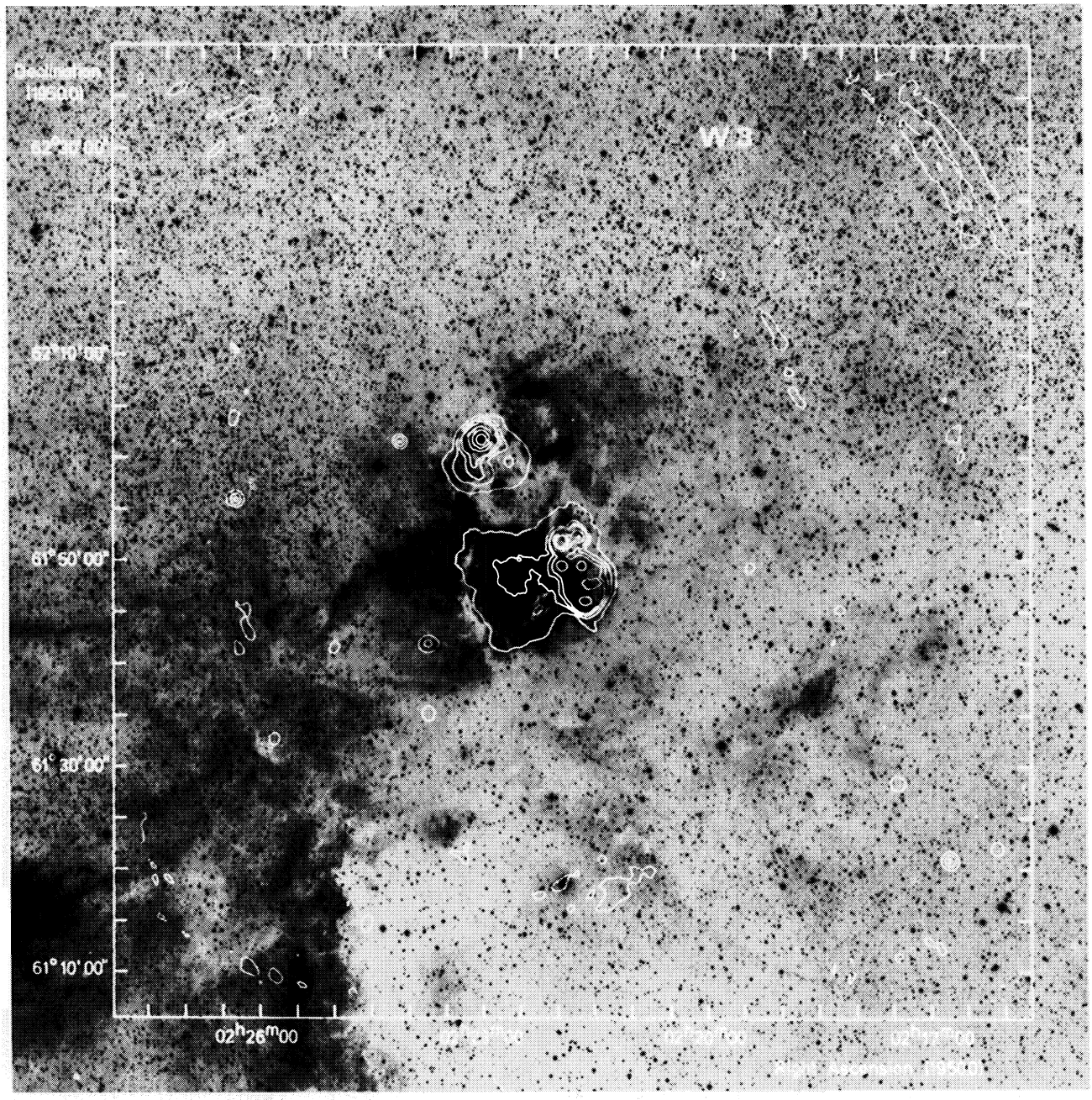

FIG. 2*b*.—Map of the continuum emission of 49 cm observed with the Westerbork Synthesis Radio Telescope (Harten 1979). The contour values are 0.050 to 0.425 Jy/beam in steps of 0.125 Jy/beam and 1.0 to 2.5 Jy/beam in steps of 0.5 Jy/beam.

TABLE 3

OBSERVATIONAL PARAMETERS FOR CS AND HCN IN W3

POSITION FROM CENTER[a]		CS (250 kHz resolution) LINE PARAMETERS					HCN (250 kHz resolution) LINE PARAMETERS				
$\Delta\alpha$ (s)	$\Delta\delta$ (arcmin)	T_A^* (K)	V_p (km s^{-1})	$\int TdV$ (K km s^{-1})	V_w (km s^{-1})	ΔV_w (km s^{-1})	T_A^* (K)	V_p (km s^{-1})	$\int TdV$ (K km s^{-1})	V_w (km s^{-1})	ΔV_w (km s^{-1})
W34	N00	≤0.3	−39.5	2			≤0.4	−36.5	2		
W25	S01	≤0.5	−41.0	2	−41.0	1.5					
W25	N01	0.3	−41.0	2							
W17	N00	1.8	−42.0	9	−42.0	7.0	1.6	−42.0	10	−42.0	6.0
							0.4	−49.0			
W17	N01	1.2	−43.5	4	−43.0	3.5					
		0.4	−39.5								
W17	N02	≤0.3	−43.0	1			≤0.3	−43.0	≤1		
W08	S01	0.8	−40.0	6	−41.5	7.0	0.8	−42.0	7	−43.5	7.0
							0.6	−45.0			
							0.4	−37.0			
W08	N00	2.4	−43.5	16	−42.5	9.0					
		0.8	−39.5								
W08	N01	1.8	−44.0	12	−43.0	8.0	2.0	−43.5	12	−43.0	8.0
		0.8	−40.0				0.6	−49.5		−49.5	3.0
							0.3	−37.0			
W08	N02	≤0.4	−44.0	1							
W08	N03	≤0.4	−41.0	2			<0.3	−45.0	≤1		
E00	S02	≤0.2	−38.0	≤1			≤0.4	−44.0	2		
E00[a]	N00	≤0.5	−40.0	4	−41.2	~7.0	1.9	−42.0	16	−40.0	25.0
							1.4	−37.5			
							0.6	−32.0?			
							0.5	−49.0?			
E00	N01	0.8	−40.0	4	−40.0	4.0					
		0.3	−45.0								
E00	N02	0.5	−40.0	3	−40.0	1.0	~0.5	−37.5	3	−37.5	7.0
		0.3	−43.0								
E17	N00	≤0.5	−39.5	2	−39.5	1.0	0.7	−38.5	6	−38.0	6.0
							0.4	−34.0			
							≤0.3	−46.5			

[a] Center at $\alpha(1950) = 02^h21^m53^s$, $\delta(1950) = +61°52'15''$.

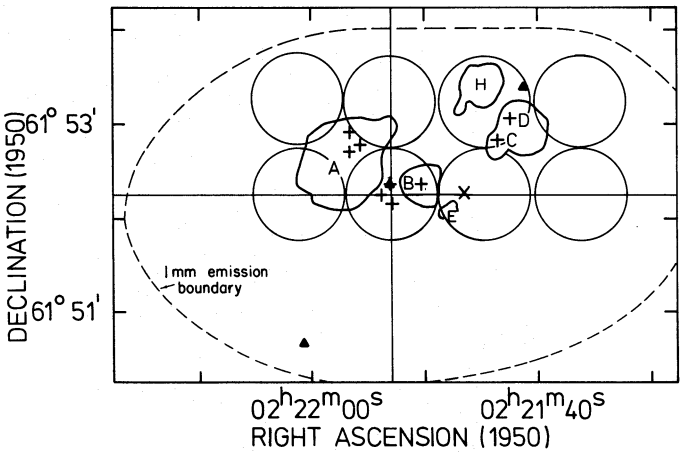

FIG. 3.—The northern group of embedded sources in the W3 core: dashed lines show the 10% level of the 1 mm emission from dust (from Westbrook *et al.* 1976), crosses indicate location of near IR sources (found by Wynn-Williams *et al.* 1972; Dyck and Simon 1977), the × marks the position of the 1720 OH maser (Wynn-Williams, Werner, and Wilson 1974), the filled triangles indicate locations of the H_2O masers (Genzel and Downes 1977), heavy solid lines outline the main radio continuum sources seen at 6 cm (from WSRT map of Harten 1980) with their letter designation (from Wynn-Williams 1971; Harris and Wynn-Williams 1976; and Harten 1980). The light solid circles show the location and size of the 1′ beam used to obtain the profiles in Fig. 5*a*. The intersection of the inner axes marks the CENTER position referred to in later figures.

TABLE 4

COMPONENTS OF W3 COMPLEX AND VICINITY

DESIGNATION	DESCRIPTION	OTHER NAMES—ASSOCIATED EMISSION	POSITION OF CENTER				REFERENCES
			l	b	α(1950)	δ(1950)	
Large scale features:	(see Fig. 1)						
Cas OB6	OB star association: $l=134°$ to $138°$, $b=-0.^{\circ}3$ to $+0.3°$	OB assoc. #43	135.°9	+1.°3	02^h39^m3	61°06′	2
W4 (radio) / IC 1805 (optical)	H II region ~1.°5 diameter	Sh 190	134.7	+0.9	02 29.5	61 13	2, 9, 15, 20, 29, 34, 36
Ocl 352 (stars)	exciting stars for W4						
W3 (radio)	H II region (see Fig. 2b)		133.8	+1.2	02 22.7	61 51	8, 9, 20, 21, 26
IC 1795 (optical)	~½° diameter				02 23.2	61 51	27, 34, 36, 38
W3 molecular cloud	molecular cloud, ~1.°5 diameter		133.4	+1.6	02 18.0	61 30	1, 6, 21, 38
Components of W3:							
W3–W4 border	includes western ionization front of W4 and eastern high intensity region of CO cloud	far-IR emission					43
W3–OH	CO condensation, includes OH and H_2O masers	IRS 8 and 9	133.°9	+1.°1	$02^h23^m16^s$	61°39′0	1, 13, 17, 21, 40, 41
AFGL 333	CO condensation with far-IR and radio emission	FIRS 5, radio #12	134.2	+0.8	02 24 37	61 14.7	11, 21, 24, 31, 34
G133.8+1.4	partly obscured H II region with some CO emission	O8 exciting star #102, radio #9	133.8	+1.4	02 23 05	62 02.0	1, 18, 23, 30
W3 main	region of brightest optical line, radio continuum and molecular emission						
W3 core	strongest CO emission, covers part of diffuse H II region and all the northern group	1 mm emission, molecular emission, far-IR emission	133.°70	+1.21	$02^h21^m46^s$	61°52′17″	1, 7, 21, 22, 33, 35, 38 11, 42
Diffuse H II region	main part of IC 1795 (Fig. 2b), extension on WSRT 50 cm map		133.8	+1.2	02 22 38	61 49.6	8, 9
N–S dust lane	at eastern edge of diffuse H II region, 15′ in δ by 1′ in α		133.9	+1.2	02 23 10	61 40–55	1
Northern group:	(see Fig. 3)						
A	shell type H II region	IRS 1, radio #8	133.72	+1.23	02 21 57	61 52 49	4, 14, 16, 18, 30, 39, 40
IRS 2	exciting stars of A		133.72	+1.22	02 21 57	61 52 41	3, 14, 40
IRS 2a			133.71	+1.22	02 21 56	61 52 44	
optical jet	Hα and [O III] emission from A		133.71	+1.23	02 21 57	61 52 52	1, 8
B	compact H II region	IRS 3	133.71	+1.21	02 21 51	61 52 21	14, 18, 30, 39, 40
C	small intense compact H II region	IRS 4, part of radio #3	133.69	+1.21	02 21 44	61 52 46	18, 28, 30, 39, 40
D	compact H II region	IRS 10, part of radio #3	133.69	+1.22	02 21 42	61 52 55	10, 18, 28, 30, 39, 40
E	small, weak radio source		133.70	+1.21	02 21 48	61 52 04	14, 16
H	H II region	radio #4	133.69	+1.23	02 21 45	61 53 30	4, 18, 38, 40

TABLE 4—*Continued*

Designation	Description	Other Names—Associated Emission	Position of Center				References
			l	b	α(1950)	δ(1950)	
H_2O maser #1 between C, D, H			133.°68	+1.°22	$02^h21^m41^s$	61°53′26″	12
IRS 5 and H_2O maser #2	massive protostar(s)	self-absorbed ^{12}CO emission, peak of 1 mm emission, strong 10 μm absorption	133.71	+1.21	02 21 53	61 52 21	1, 7, 12, 14, 19, 35 37, 40
IRS 6	20 μm IR source		133.71	+1.21	02 21 54	61 52 16	40
IRS 7	compact H II region		133.71	+1.21	02 21 53	61 52 10	49
1720 OH maser			133.70	+1.21	02 21 46	61 52 17	14, 32, 41
5 cm OH absorption			133.68	+1.20	−2 21 35	61 52 23	25
Southern group:	(see Fig. 2*b*)						
radio #7	compact H II region		133.73	+1.18	02 21 57	61 50 06	4, 18, 28, 30
H_2O maser #3 NE of radio #7			133.74	+1.20	02 22 06	61 50 40	5, 12
radio #2	compact H II region		133.70	+1.17	02 21 41	61 50 12	4, 18, 28, 30
radio #6		IR cluster	133.73	+1.15	02 21 51	61 48 10	4, 18, 28, 30
NGC 896	partly obscured H II region	radio #1	133.72	+1.11	02 21 38	61 46 36	4, 9, 18, 28, 30

REFERENCES

1. This paper.
2. Alter, Ruprecht, and Vanýsek 1970.
3. Beetz, Elsässer, and Weinberger 1974.
4. Beetz *et al.* 1976.
5. Cesarsky *et al.* 1978.
6. Dickel 1973.
7. Dickel *et al.* 1975.
8. Dickel and Harten 1980.
9. Dreyer 1910.
10. Dyck and Simon 1977.
11. Fazio *et al.* 1975.
12. Genzel and Downes 1977.
13. Goss, Lockart, and Fomalont 1975.
14. Hackwell *et al.* 1978.
15. Hagen 1970.
16. Harris and Wynn-Williams 1976.
17. Harten 1976.
18. Harten 1980.
19. Hills *et al.* 1972.
20. Ishida and Kawajiri 1968.
21. Lada *et al.* 1978.
22. Morris *et al.* 1974.
23. Ogura and Ishida 1976.
24. Price and Walker 1976.
25. Rickard, Zuckerman, and Palmer 1975.
26. Schmitter 1971.
27. Schraml and Mezger 1969.
28. Schultz, Proetel, and Schmidt 1978.
29. Sharpless 1959.
30. Sullivan and Downes 1973.
31. Thronson, Harvey, and Gatley 1979.
32. Turner 1970.
33. Turner and Gammon 1975.
34. Wendker and Altenhoff 1977.
35. Westbrook *et al.* 1976.
36. Westerhout 1958.
37. Willner 1977.
38. Wilson *et al.* 1979.
39. Wynn-Williams 1971.
40. Wynn-Williams, Becklin, and Neugebauer 1972.
41. Wynn-Williams, Werner, and Wilson 1974.
42. Werner *et al.* 1980.
43. Thronson, Campbell, and Hoffmann 1979.

remainder of the surrounding cloud is at $\sim -43 \pm 1$ km s^{-1}. The $\pm$ values refer to a typical range in velocities, not to their errors. The LSR velocities of the optically visible ionized hydrogen are similar to the molecular velocities: Georgelin and Georgelin (1976) find an *average* velocity of -40.7 km s^{-1} toward W3 and -46 km s^{-1} toward W4. The eastern edge of the radio continuum emission associated with W3 coincides with the prominent, narrow north-south dust lane which separates the faint Hα emission of W4 to the east from the bright Hα emission of W3 to the west (refer to Fig. 2). Along this same boundary, ^{12}CO emission is detected at both velocities, -40 km s^{-1} and -46 km s^{-1}. The average velocity of the stars in the open cluster Ocl 352 which excite W4 is -34 km s^{-1} (Hagen 1970). This significant difference in the velocity of the stars compared to that of the molecular and ionized gas may be the result of passage through a galactic shock and later expansion of the W4 H II region as will be described in the subsequent paper.

c) *The W3 Complex*

i) *Distribution of the* ^{12}CO *Emission*

As mentioned in § III*b*(ii), the strongest ^{12}CO emission comes from the W3 core (see Fig. 2*a*). Figure 2*a* shows all the details of the distribution of T_A*(^{12}CO) which are apparent with our sampling grid and the 1′ and 2′ beams. The central part with T_A*(^{12}CO) $\gtrsim$ 17 K coincides with the region of 1 mm emission (Westbrook *et al.* 1976) outlined in Figure 3, and with the region of high-far-infrared surface brightness (Fazio *et al.* 1975; Werner *et al.* 1980). The 30 K contour is centered close to compact H II region C, and includes most of the "northern group" of sources which are drawn as heavy lines in Figure 3 (from the 6 cm radio continuum data of Harten 1980). The maximum observed ^{12}CO temperature is 31 K; because of the universal 2.7 K background radiation, the minimum kinetic temperature needed to produce this is 35 K. Thus *the kinetic temperature must be greater than or equal to* 35 K *in at least part of the cloud.* By contrast the dust temperature over the central few arc minutes of the W3 core lies in the range 60–90 K (Werner *et al.* 1980).

The CO emission extends to the partly obscured H II region G133.8+1.4 which lies 16′ to the northeast of C, but falls off sharply in the direction of the "southern group" of H II regions listed in Table 4 (compare Figs. 2*a* and 2*b*). *This apparent cutoff suggests that there is a physical boundary between the* CO *cloud* (*W3 core*) *and this southern group of sources.* The 21 cm continuum map (Harten 1980) also shows a distinct break between the northern and southern group. To the east, the CO emission covers much of the optical, diffuse H II region IC 1795, but some of this CO emission probably comes from behind the H II region. Otherwise, one would not expect the H II region to be so bright optically in the presence of the accompanying extinction associated with the molecular cloud.

ii) *Line Shapes and Widths*

The molecular lines are asymmetrical and broad where the CO emission is strongest, i.e., within the region of the 1 mm dust emission and toward the embedded sources of excitation shown in Figure 3. The ^{12}CO and ^{13}CO profiles for this area are shown in Figures 4*a* and 4*b*. The position labeled CENTER is at the intersection of the inner axes in Figure 3 toward the group of near-infrared sources IRS 5, 6, and 7 where the 1 mm emission and the ^{13}CO emission have their maximum intensities. It is toward CENTER and 8^s east of it that we find the *self-absorbed* ^{12}CO *profiles* (Dickel *et al.* 1975). The fact that the peak of the ^{13}CO emission falls in the region of the dip in the ^{12}CO profile indicates that this is indeed self-absorption, not a second velocity component in the ^{12}CO profile. Figure 5*a* displays the profiles of ^{12}CO, ^{13}CO, HCN, and CS observed toward the inner eight positions indicated by the circular beams in Figure 3. The self-absorption dip in the ^{12}CO profile toward IRS 5–7 is displaced about 1½ km s^{-1} toward the positive velocities relative to the velocity of the peak of the ^{13}CO emission. The profiles at neighboring positions are asymmetric, with the more gradual slope of the ^{12}CO line usually on the positive velocity side of the line; we have interpreted this to mean that there is incipient self-absorption throughout the region. The midpoint of the base of these lines is centered close to the peak of the ^{13}CO emission. These facts mean that *foreground material which is just becoming optically thick* (*with* $\tau_{^{12}CO} \sim 3$) *is moving away from the observer by a few* km s^{-1} *relative to the bulk of the material which forms the core of the line.* Since the ^{13}CO line does not show self-absorption effects, $\tau_{^{13}CO} < 1$.

The CS ($J = 2$–1) *lines have asymmetric shapes similar to the* ^{12}CO *lines:* the CS emission extends just as far as the ^{13}CO emission in the direction of positive velocities but well beyond the edge of the ^{13}CO emission profile for more negative velocities. Most of the CS lines shown in Figure 5*a* have T_A* of the peak emission between 1 and 2.5 K (note that both the CS and HCN profiles in Fig. 5*a* have been multiplied by a factor of 10). However, toward IRS 5–7 the CS emission has fallen to $\sim$0.5 K, where it is nearly lost in the noise. We feel that this effect is real since the positions IRS 5–7, and E17 (see Table 3) were observed in CS at the same air mass and within 25 minutes of the CS observations at the positions N1W8 and W17.

The HCN ($J = 1$–0) line has three hyperfine components: the $F = 2$–1 line is the strongest; the $F = 1$–1 line has a frequency shift equivalent to $\sim +5$ km s^{-1} from the $F = 2$–1 line and should be about 60% as intense for an optically thin, LTE situation; and the $F = 0$–1 line at ~ -7 km s^{-1} should be about 20% as intense. The intensities of the hyperfine lines may well be in the proper LTE ratios for weak lines away from the center (e.g., E17 and W08S01 in Table 3), but the low signal-to-noise precludes an accurate assessment here. However, where the lines are stronger such as toward positions N1W8 and W17 the intensity

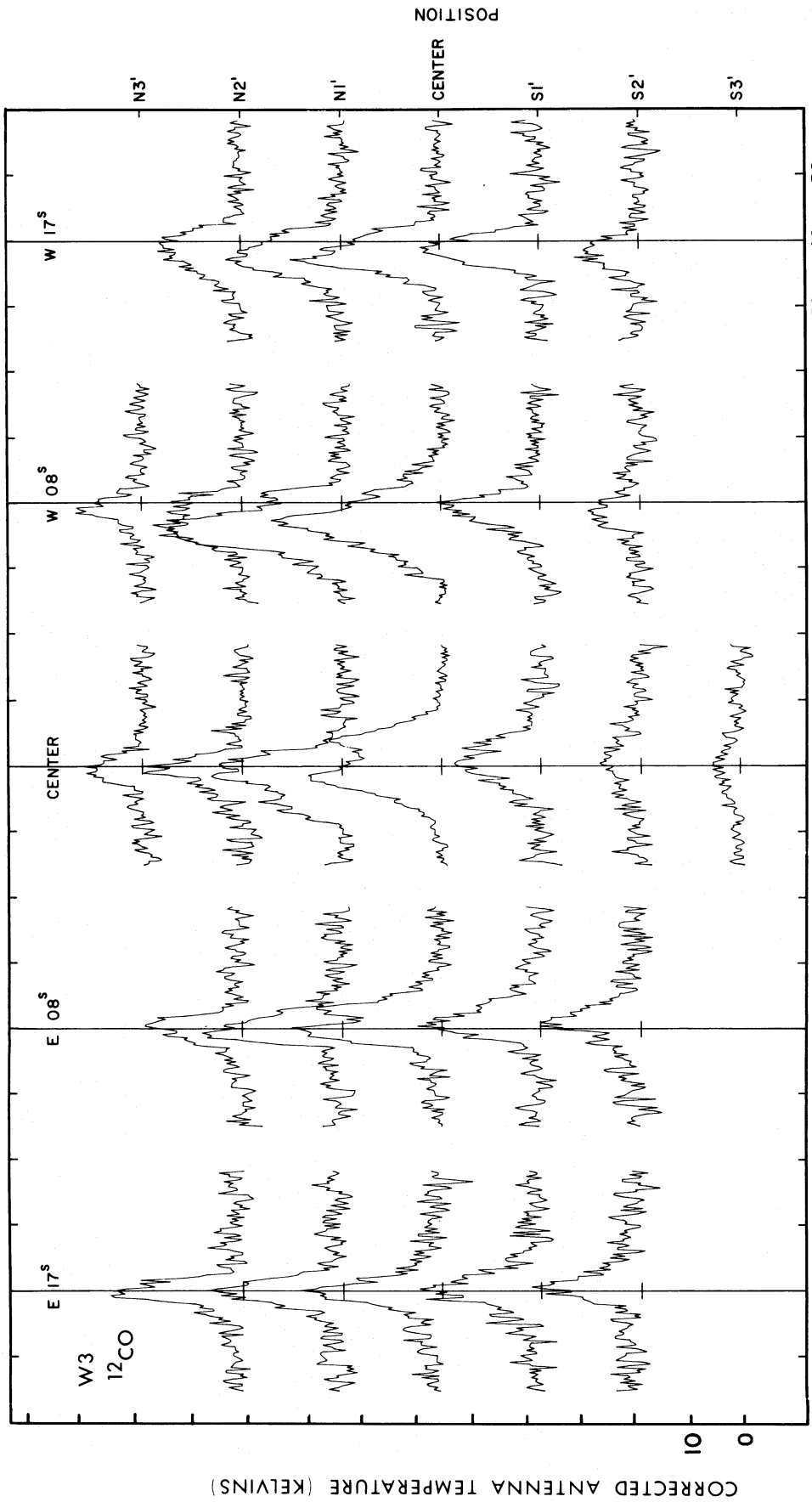

FIG. 4a

FIG. 4.—(*a*), (*b*) Profiles of the CO emission from the region shown in Fig. 3. The individual profiles are spaced according to the right ascension and declination relative to CENTER as indicated by the top and right-hand axes. The CENTER position is toward IRS 5–7 at $\alpha(1950) = 02^h21^m53^s$ and $\delta(1950) = +61°52'15''$. The frequency resolution is 100 kHz, and the spatial resolution is 70″. (*a*) ^{12}CO: the interval of corrected antenna temperature between tick marks on the left-hand axis is 10 K. (*b*) ^{13}CO: the interval of corrected antenna temperature between the tick marks on the left-hand axis is 5 K.

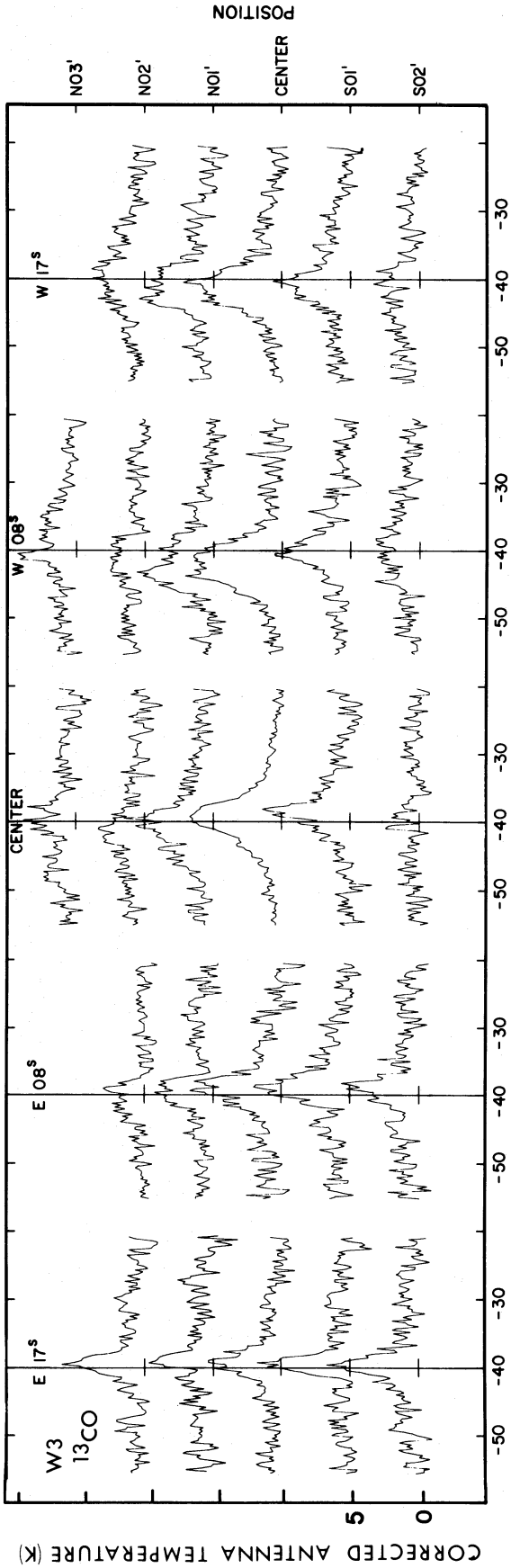

FIG. 4b

FIG. 4.—*Continued*

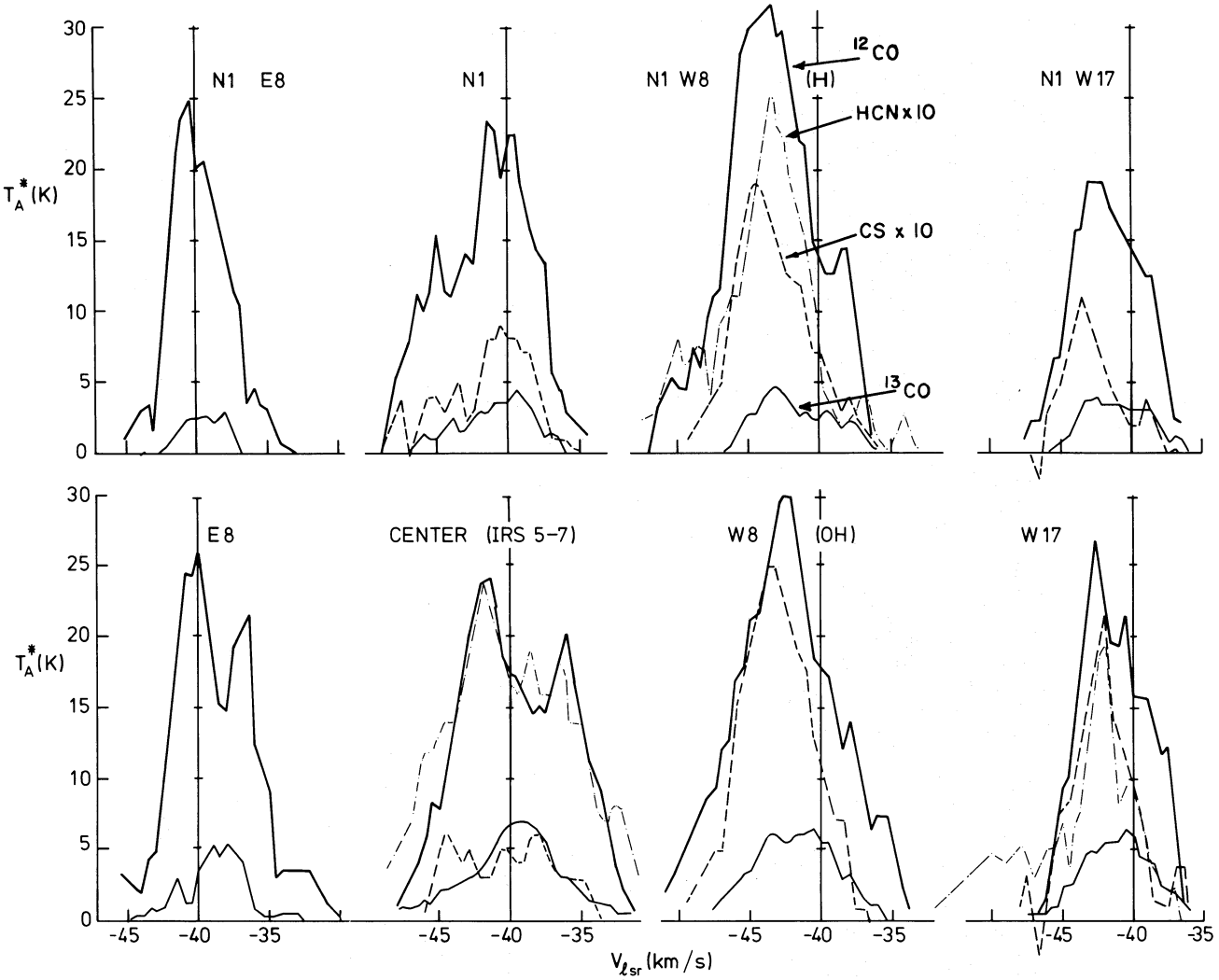

FIG. 5a

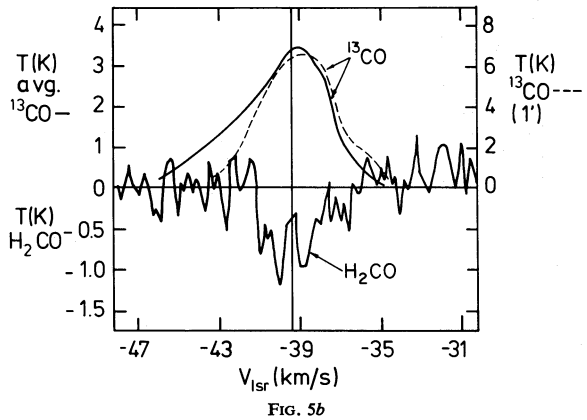

FIG. 5b

FIG. 5a.—Line profiles toward the positions marked by the light circles in Fig. 3. Each profile is labeled with its position in arcminutes north and/or seconds of time east or west of the CENTER. The main excitation sources within the beam are given in the parentheses. The ^{12}CO profiles are drawn by (tall) dark solid lines, the ^{13}CO profiles by (low) light solid lines, the CS profiles by dashed lines, and the HCN profiles by light dot-dashed lines. The temperature scale for ^{12}CO and ^{13}CO is marked in 5 K intervals along the vertical axis; for CS and HCN the numbers must be divided by 10 to obtain the temperature (0.5 K intervals). The vertical axis within each profile is at a radial velocity of -40 km s^{-1}, and 5 km s^{-1} intervals are marked along the horizontal axis.

FIG. 5b.—The ^{13}CO emission profile observed with a velocity resolution of $\sim\frac{1}{4}$ km s^{-1} and spatial resolution of $\sim 1'$ toward the CENTER position (*dashed line*), the Gaussian-weighted average of the ^{13}CO emission profiles within a circle of diameter 5.'8 centered on this position (*solid line*), and the corresponding H_2CO absorption profile at 6 cm, (line antenna temperature) observed with a velocity resolution of $\sim\frac{1}{4}$ km s^{-1} and spatial resolution $\sim 6.'6$.

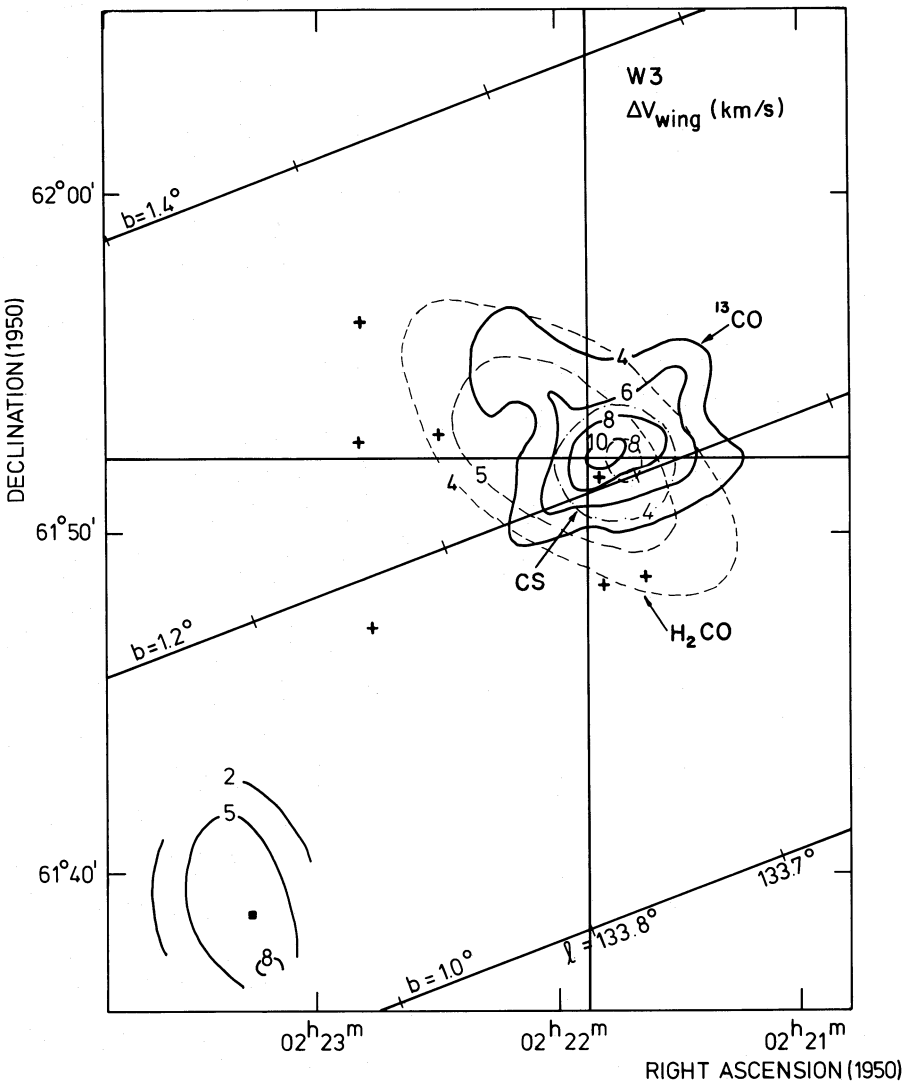

FIG. 6.—Line widths in km s^{-1}, ΔV_w, toward W3: ^{13}CO widths at the $T_A^* \sim 1$ K level (*solid lines*), H_2CO widths at the $|T_A| \sim 0.25$ K level (*dashed lines*), and CS widths at the $T_A^* \sim 0.5$ K level (*dot-dashed lines*). For this and the following figures, the intersection of the inner axes marks the position of the CENTER at $\alpha(1950) = 02^h21^m53^s$ and $\delta(1950) = +61°52'15''$, lines of constant galactic latitude are labeled, and the crosses indicate the positions of reference stars.

of the $F = 0$–1 hyperfine line is equal to or slightly greater than the optically thin LTE value whereas the $F = 1$–1 line is down by a factor of 4 or more (refer to Fig. 5*a* and Table 3). This behavior, which is typical of other molecular clouds, is not yet fully understood (e.g., Kwan and Scoville 1975; Gottlieb *et al.* 1975). The HCN ($F = 2$–1) line is centered nearer to the peak rather than the midpoint velocity of the overall ^{12}CO profile (refer to profiles at positions N1W8 and W17 in Figure 5*a*). *Toward IRS 5–7 where the* CS *emission is weak, the* HCN *emission remains high and the line shape is almost identical to that of the* ^{12}CO.

The H_2CO profile (obtained with a 6'.6 beam and 0.24 km s^{-1} velocity resolution by Dickel 1973) is shown in Figure 5*b* along with two ^{13}CO emission profiles (with 0.27 km s^{-1} resolution): the dashed curve is for a 1' beam centered on IRS 5–7, and the solid curve is the Gaussian-weighted average of the ^{13}CO profiles within a circle of diameter 5'.8 centered on this position. This is nearly the same as the 6'.6 HPBW observing beam used for the H_2CO observations. The H_2CO absorption profile at 6 cm toward IRS 5–7 looks remarkably like the ^{13}CO emission profile in both velocity and line width, so both lines are sampling nearly the same material along the line of sight. Since the H_2CO line is seen in absorption, its profile is governed mainly by the material in front of the continuum sources. Both the 6 cm H_2CO profile in Figure 5*b* and the 2 cm one of Evans *et al.* (1975, with resolutions of 1' and 1 km s^{-1}) are asymmetric, with the line being steeper on the negative-velocity side. The excess gas at the most negative velocities seen in emission in the average ^{13}CO profile but missing from

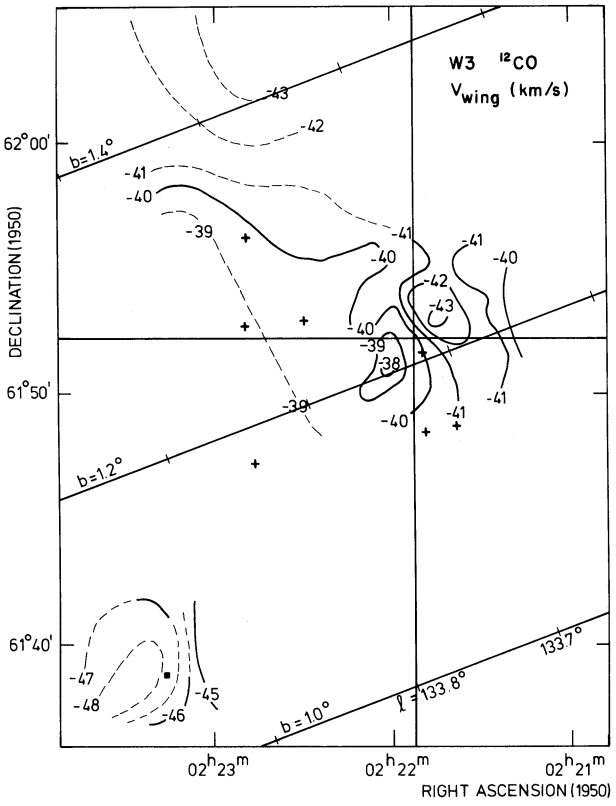

FIG. 7a

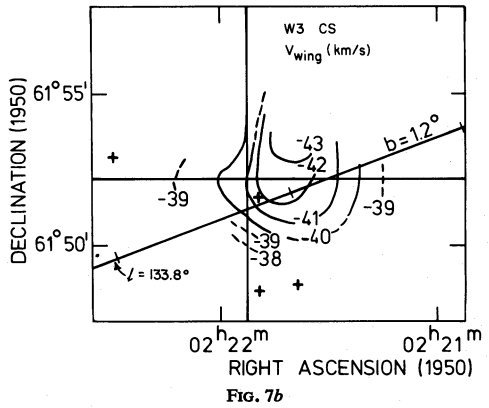

FIG. 7b

FIG. 7.—The distribution of midpoint velocities in km s^{-1}, V_w, toward W3. Dashed lines indicate uncertain location of the contour. (*a*) ^{12}CO. (*b*) CS.

the H_2CO profiles is most likely located behind the continuum sources in the rear of the cloud, which mean that the back of the cloud is moving toward the observer relative to the bulk of the material. Since the foreground material and background material are moving toward each other, the cloud is collapsing.

In addition to the missing H_2CO gas at the most negative velocities, there may be an emission component near the middle of the absorption line which could be responsible for some of the asymmetry such as seen toward NGC 7538 by Downes and Wilson (1974). Current observations of H_2CO at 6 cm with the Westerbork Synthesis Radio Telescope (by H. Dickel and collaborators) should allow us to see the structure of the profile at various positions within the cloud.

All the molecular lines are wider toward the embedded excitation sources as seen in Figure 6 in which the inner axes intersect at the CENTER position. To avoid the problems introduced by asymmetries, the width, ΔV_w, was measured in the wings of the lines at the base of the profile just above the noise levels as described in the figure legend. The HCN line widths are not included because of the complicating hyperfine structure. Although the CS and HCN lines are generally narrower than the CO lines, the $F = 2$–1 hyperfine line of HCN is just as broad as the ^{12}CO line at IRS 5–7 (compare the profiles at N1W8 and CENTER in Fig. 5*a*).

Since the nature of both the ^{12}CO self-reversal and the H_2CO absorption compared to the ^{13}CO emission are consistent with an overall collapse of the molecular core, part of the increased line width toward the center of the cloud is probably due to this collapse motion. However, in the outskirts of the cloud (in the plane of the sky), the observed line widths should be dominated by turbulent motion. If v_t is the turbulent velocity (as defined by Leung 1978) and ΔV is the observed full width at half-intensity, then for an optically thin gas such as ^{13}CO with $0 < \tau < 1$, $1.7v_t < \Delta V < 2.5v_t$ (Leung and Liszt 1976; Leung 1978). In the outer parts of the cloud, $\Delta V(^{13}CO) \approx 3$–4 km s^{-1}, so the *turbulent velocity is on the order of* 2 km s^{-1}.

iii) *Velocities*

In trying to unravel the dynamics in the W3 region, we must consider that the observed radial velocities across the cloud are a composite of the motion of the cloud as a whole in the spiral arm, hereafter referred to as the "rest velocity," and systematic motions within the cloud due to such processes as collapse or rotation. If a cloud has uniform temperature and density, the velocity of the peak of the emission line, V_p, would be the average velocity of the gas along the line of sight, and the rest velocity would be the V_p observed in the direction of the cloud center. In the midst of nonuniformities which can seriously shift the V_p of an optically thick or thin line away from the (unweighted) average velocity of the gas along a particular line of sight, we feel that a better measure of this average velocity is V_w, which is the radial velocity of the midpoint of the line measured near the base of the profile.

The midpoint velocity, V_w, for the ^{12}CO (from col. [7] of Table 2) is plotted in Figure 7*a*. *The rest velocity of the W3 core is around* -40.5 km s^{-1}, *but there is a gradient in the average radial velocity* in the core of the ^{12}CO emission from -38 km s^{-1} in the southeast to -43 km s^{-1} in the northwest (with the maximum effect roughly along a line connecting the three H_2O masers tabulated by Genzel and Downes 1977; see Table 4). Although the exact velocities differ, the same trend is observed for CS (Fig. 7*b*), ^{13}CO, and

HCN as well, irrespective of whether the peak or midpoint velocity is plotted. The contours of Figure 7*a* might suggest solid-body rotation with a period of about 10^6 years for an embedded region perhaps 2 pc across (at a distance of 2 kpc). In the subsequent paper, evidence for and against such a rotation is presented and an alternative set of circumstances is suggested to explain the gradient.

iv) ^{13}CO *Optical Depths and the Velocity of the Absorbing* ^{12}CO *Gas*

The optical depth at the center of the $J = 1$–0 line of ^{13}CO, $\tau(^{13}\mathrm{CO})$, would be equal to r, the ratio of the ^{13}CO intensity to the ^{12}CO intensity, under conditions of LTE and small r. Therefore, the distribution of r is an indication of the variation of τ. The values of maximum r in column (14) of Table 2B have been multiplied by 100 and plotted in Figure 8*a* with an uncertainty of ~ 5 units due to uncertainties in the location of the ^{13}CO baselines. As usual the intersection of the inner axes in Figure 8*a* marks the CENTER position. The "northern group" of compact H II regions is located mainly to the north of the inner horizontal axis, and the "southern group" begins at and extends to the south of the line representing galactic latitude $b = 1\overset{\circ}{.}2$. One sees that max r, and thus *the optical depth of the* ^{13}CO *line, is highest just in the region between the northern and southern group. Another maximum occurs in the southeast in the region of the W3–OH maser which is marked by the filled square.*

The velocity where the ratio within the profile is a maximum, V_r, is a density-weighted mean of the velocity of the CO gas along the line of sight so that V_r is close to $V_p(^{13}\mathrm{CO})$. However, where self-absorption effects occur in the ^{12}CO line, V_r will be closer to the velocity of the gas which is just becoming optically thick (since the ^{12}CO dip or shoulder is usually displaced 1 or 2 km s^{-1} from the ^{13}CO peak as mentioned in § III*c*[ii]). The velocity V_r (in col. [15] of Table 2B) has been plotted in Figure 8*b*. It is not well defined to the northwest of CENTER (hatched area) because the optical depth is fairly uniform with $r \lesssim 0.2$ across the profile between -39 km s^{-1} to -43 km s^{-1}. The variation in V_r seen in Figure 8*b* is similar to that seen for the midpoint velocities in Figures 7*a* and 7*b*. In *the southeast where the optical depths are higher, we find* (1) *the (density-weighted) velocity* V_r *is* 1 *to* 2 km s^{-1} *more positive than the mean velocity of* ^{12}CO, V_w; (2) *the lines of constant velocity run parallel to the edge of the diffuse* H II *region; and* (3) *the most positive velocities* (~ -38 km s^{-1}) *are along the border with the diffuse*

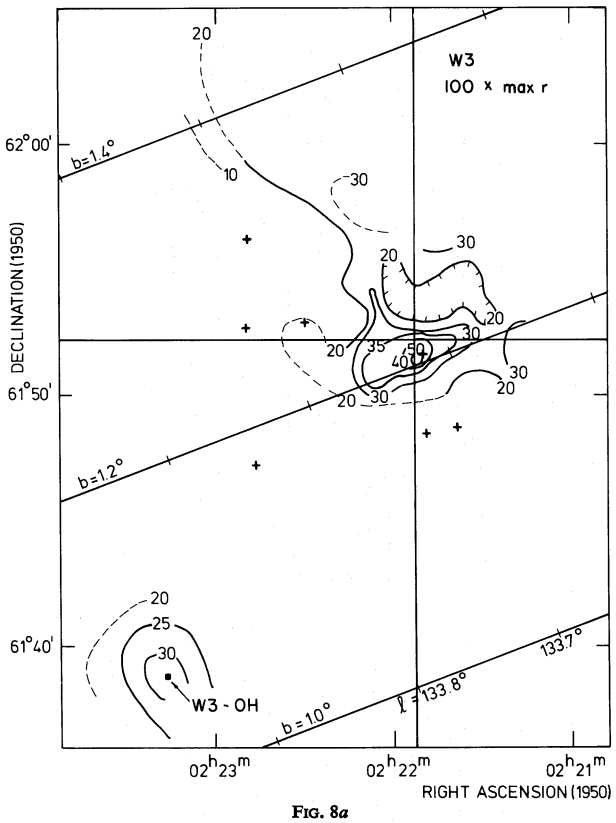

FIG. 8*a*

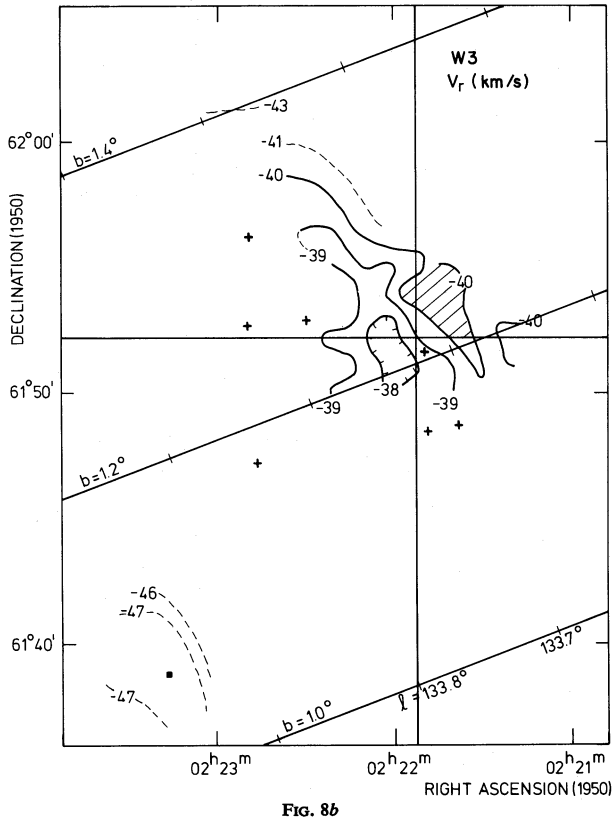

FIG. 8*b*

FIG. 8.—(*a*) The distribution of 100 (max r) toward W3 where (max r) is the maximum value across the profile of the ratio of the ^{13}CO intensity to the ^{12}CO intensity. Dashed lines indicate uncertain location of the contour. As discussed in the text, this shows the approximate distribution of the optical depth in the ^{13}CO line. (*b*) The distribution of V_r (the velocity where the intensity ratio of ^{13}CO to ^{12}CO across the profile has a maximum). Dashed lines indicate uncertain location of the contour. Contours of V_r are not plotted within the hatched area because they are ill determined there.

H II *region*. These findings are important for the overall interpretation of the dynamics in the W3 core presented in the subsequent paper.

v) *Distributions of* CS *and* HCN *Emission*

Both the CS and HCN emission are confined to the central region of W3 where the ^{12}CO lines are asymmetric (see Fig. 9). The presence of the emission from these high-excitation molecules and the high column densities of dust and gas determined from 1 mm emission and CO emission coupled with the small size of the W3 core indicate that *the average molecular hydrogen density is at least* 10^4 cm^{-3} there. Furthermore, there must be *changes in density* from perhaps 10^3 cm^{-3} where the HCN and 1 mm emission fall below detection to possibly 10^5 where the HCN molecules are excited and, of course, to locally much higher values in the vicinity of the maser sources. In Figure 9 the integrated brightness is plotted so that it includes the emission from all the hyperfine components of HCN. One sees that the maximum integrated brightness for HCN is toward IRS 5–7, where the peak in the 1 mm emission implies that density is highest. In the western half of the core, the values of integrated brightness (and also the temperature at the peak of the line) are similar for CS and HCN. However, *in the eastern part, the integrated brightness of* CS *is much weaker while that of* HCN *remains strong*. Since, for the same molecular densities, the intensities of the CS (J = 2–1) and HCN (J = 1–0, F = 2–1) lines should be quite similar, one expects very similar intensity distributions with the maximum emission for both CS and HCN occurring where the density is highest toward IRS 5, but the CS maximum is 8^s to the west. *Thus, the observed variation in the relative intensities suggest a variation in the abundance of* CS *within the W3 cloud*. This is discussed in more detail in the subsequent paper.

IV. SUMMARY

The W3 complex includes a wide variety of objects with different sizes, ages, and types of emission from young, dust-embedded possible protostellar objects to older, diffuse H II regions which are seen optically. Maps of the distribution of the emission from the J = 1–0 transition of ^{12}CO and ^{13}CO, the J = 2–1 transition of CS, and the J = 1–0 transition of HCN have been presented which show the "core" of the W3 molecular cloud (Fig. 3) to be a dense and dynamically active region. Pronounced self-absorption is seen in the ^{12}CO profile toward IRS 5 and to a lesser degree

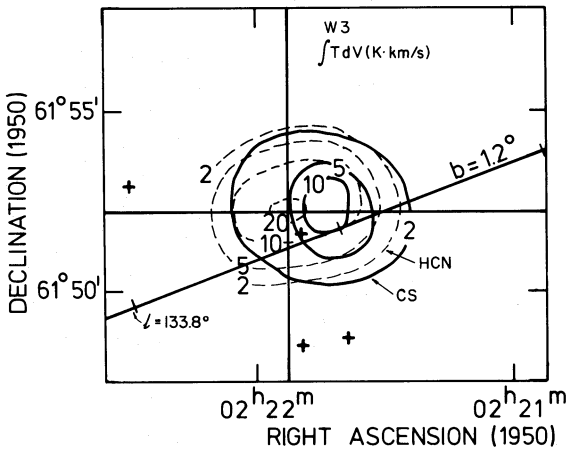

FIG. 9.—Integrated brightnesses $\int TdV$ in K·km s^{-1} for CS (*solid lines*) and HCN (*dashed lines*).

throughout the core. The maximum ^{12}CO emission is towards the compact H II region C. The ^{13}CO and HCN emission peak at the position of IRS 5, whereas the CS emission peaks 8^s to the west in the direction of the 1720 OH maser. Emission from both HCN and CS is confined to the inner region where the 1 mm emission from dust is strongest and the ^{12}CO profiles are asymmetric. The W3 core as a whole appears to be collapsing. Additional systematic motions occur close to the border with IC 1795. The physical parameters which have been determined from the data here will be used in the next paper (Dickel, 1980) to develop a model of the W3 molecular cloud to explain some of these puzzling observational features.

We thank N. Z. Scoville, R. B. Pomphrey, and J. D. White for help with the observations. The Aerospace spectral line radio astronomy program was supported jointly by the National Science Foundation grant MPS-73-04554 and the Aerospace Corporate Programs for Research and Investigation. The NRAO is operated by Associated Universities, Inc., under contract with the National Science Foundation. The research of H. R. D. was partially supported by NSF grants AST 75-22208 and AST 77-21021. J. R. D. acknowledges a Fulbright-Hays travel award from the Netherlands-America Commission for Educational Exchange. H. R. D. and J. R. D. enthusiastically acknowledge the hospitality and support of the Sterrewacht te Leiden.

REFERENCES

Alter, G., Ruprecht, J., and Vanýsek, V. 1970, in *Catalogue of Star Clusters and Associations*, ed. G. Alter, B. Balázo, and J. Ruprecht (Budapest: Akadémiai Kiadó).
Beetz, M., Elsässer, H., Poulakos, C., and Weinberger, R. 1976, *Astr. Ap.*, **50**, 41.
Beetz, M., Elsässer, H., and Weinberger, R. 1974, *Astr. Ap.*, **34**, 335.
Cesarsky, C. J., Cesarsky, D. A., Churchwell, E., and Lequeux, J. 1978, *Astr. Ap.*, **68**, 33.
Dickel, H. R. 1973, in *IAU Symposium 52, Interstellar Dust and Related Topics*, ed. J. M. Greenberg and H. C. van de Hulst (Dordrecht: Reidel), p. 277.
Dickel, H. R. 1980, *Ap. J.*, in press (sequel to this papcr).
Dickel, H. R., Dickel, J. R., and Wilson, W. J. 1977, *Ap. J.*, **217**, 56 (Paper I).
Dickel, H. R., Dickel, J. R., Wilson, W. J., and Pomphrey, R. B. 1975, *Bull. AAS*, **7**, 556.
Dickel, H. R., and Harten, R. 1980, in preparation.
Dickel, J. R., Dickel, H. R., and Wilson, W. J. 1978, *Ap. J.*, **223**, 840 (Paper II).
Downes, D., and Wilson, T. L. 1974, *Ap. J.* (*Letters*), **191**, L77.
Dreyer, J. L. E. 1910, *Mem. R.A.S.*, **59**, 114.
Dyck, H. M., and Simon, T. 1977, *Ap. J.*, **211**, 421.

Evans, N. J., Zuckerman, B., Morris, G., and Sato, T. 1975, *Ap. J.*, **196**, 433.
Fazio, G. G., Kleinmann, D. E., Noyes, R. W., Wright, E. L., Zeilik, M., II, and Low, F. J. 1975, *Ap. J.* (*Letters*), **199**, L177.
Forster, J. R., Welch, W. J., and Wright, M. C. H. 1977, *Ap. J.* (*Letters*), **216**, L121.
Genzel, R., and Downes, D. 1977, *Astr. Ap. Suppl.*, **30**, 145.
Georgelin, Y. M., and Georgelin, Y. P. 1976, *Astr. Ap.*, **49**, 57.
Goss, W. M., Lockhart, I. A., and Fomalont, E. B. 1975, *Astr. Ap.*, **40**, 439.
Gottlieb, C. A., Lada, C. J., Gottlieb, E. W., Lilley, A. E., Litvak, M. M. 1975, *Ap. J.*, **202**, 655.
Hackwell, J. A., Gehrz, R. D., Smith, J. R., and Briotta, D. A. 1978, *Ap. J.*, **221**, 797.
Hagen, G. 1970, *Pub. DDO*, Vol. **4**.
Harris, S., and Wynn-Williams, C. G. 1976, *M.N.R.A.S.*, **174**, 649.
Harten, R. 1976, *Astr. Ap.*, **146**, 109.
———. 1980, in preparation.
Hills, R., Janssen, M. A., Thornton, D. D., and Welch, W. J. 1972, *Ap. J.* (*Letters*), **175**, L59.
Ishida, K. 1969, *M.N.R.A.S*, **144**, 55.
———. 1970, *Pub. Astr. Soc. Japan*, **22**, 277.
Ishida, K., and Kawajiri, N. 1968, *Pub. Astr. Soc. Japan*, **20**, 95.
Kwan, J., and Scoville, N. Z. 1975, *Ap. J.* (*Letters*), **195**, L85.
Lada, C. J., Elmegreen, B. G., Cong, H.-Ih., and Thaddeus, P. 1978, *Ap. J.* (*Letters*), **226**, L39.
Leung, C. M. 1978, *Ap. J.*, **225**, 427.
Leung, C. M., and Liszt, H. S. 1976, *Ap. J.*, **208**, 732.
Morris, M., Palmer, P., Turner, B. E., and Zuckerman, B. 1974, *Ap. J.*, **191**, 349.
Ogura, K., and Ishida, K. 1976, *Publ. Astr. Soc. Japan*, **28**, 651.
Price, S. D., and Walker, R. G. 1976, *The AFGL Four Color Infrared Sky Survey* (Washington: GPO AFGL-TR-0208).
Rickard, L. J, Zuckerman, B., and Palmer, P. 1975, *Ap. J.*, **200**, 6.
Rogers, A. E. E., Moran, J. M., Crowther, P. P., Burke, B. F., Meeks, M. L., Ball, J. A., and Hyde, G. M. 1967, *Ap. J.*, **147**, 369.
Rohlfs, K., Braunsfurth, E., and Hills, D. L. 1977, *Astr. Ap. Suppl.*, **30**, 369.
Schmitter, E. F. 1971, *A.J.*, **76**, 571.
Schraml, J., and Mezger, P. G. 1969, *Ap. J.*, **156**, 269.
Schultz, A., Proetel, K., and Schmidt, Th. 1978, *Astr. Ap.*, **64**, L13.
Sharpless, S. 1959, *Ap. J. Suppl.*, **4**, 257.
Sullivan, W. T., III, and Downes, D. 1973, *Astr. Ap.*, **29**, 369.
Thronson, H. A., Campbell, M. F., and Hoffmann, W. F. 1979, preprint.
Thronson, H. A., Harvey, P. M., and Gatley, I. 1979, *Ap. J.* (*Letters*), **229**, L133.
Turner, B. E. 1970, *Ap. Letters*, **6**, 99.
Turner, B. E., and Gammon, R. H. 1975, *Ap. J.*, **198**, 71.
Ulich, B. L., and Haas, R. W. 1976, *Ap. J. Suppl.*, **30**, 247.
Wendker, H. J., and Altenhoff, W. J. 1977, *Astr. Ap.*, **54**, 301.
Werner, M. W., Becklin, E. E., Gatley, I., Harper, D. A., Lowenstein, R., Mosley, H., Neugebauer, G., Sellgren, K., and Thronson, H. A. 1980, in preparation.
Westbrook, W. E., Werner, M. W., Elias, J. H., Gezari, D. Y., Hauser, M. G., Lo, K. Y., and Neugebauer, G. 1976, *Ap. J.*, **209**, 94.
Westerhout, G. 1958, *BAN*, **14**, 215.
Willner, S. P. 1977, *Ap. J.*, **214**, 706.
Wilson, W. J., Schwartz, P. R., Epstein, E. E., Johnson, W. A., Etcheverry, R. D., Mori, T. T., Berry, G. G., and Dyson, H. B. 1974, *Ap. J.*, **191**, 357.
Wynn-Williams, C. G. 1971, *M.N.R.A.S.*, **151**, 397.
Wynn-Williams, C. G., Becklin, E. E., and Neugebauer, G. 1972, *M.N.R.A.S.*, **160**, 1.
Wynn-Williams, C. G., Werner, M. W., and Wilson, W. J. 1974, *Ap. J.*, **187**, 41.

HÉLÈNE R. DICKEL and JOHN R. DICKEL: Astronomy Department, University of Illinois, 341 Astronomy Building, 1011 W. Springfield Avenue, Urbana, IL 61801

MICHAEL W. WERNER: Division of Physics, Mathematics and Astronomy, California Institute of Technology, Downes Laboratory 320-47, Pasadena, CA 91125

WILLIAM J. WILSON: Electronics Research Laboratory, Aerospace Corporation A6/2457, Box 92957, Los Angeles, CA 90009